Comparison of prone versus supine 18F-FDG-PET of locally advanced breast cancer: Phantom and preliminary clinical studies

Jason M. Williams, Sudheer D. Rani, and Xia Li
Institute of Imaging Science, Vanderbilt University, Nashville, Tennessee 37232 and Department of Radiology and Radiological Sciences, Vanderbilt University, Nashville, Tennessee 37232

Lori R. Arlinghaus
Institute of Imaging Science, Vanderbilt University, Nashville, Tennessee 37232

Tzu-Cheng Lee
Department of Bioengineering, University of Washington, Seattle, Washington 98195

Lawrence R. MacDonald and Savannah C. Partridge
Department of Radiology, University of Washington, Seattle, Washington 98195

Hakmook Kang
Institute of Imaging Science, Vanderbilt University, Nashville, Tennessee 37232 and Department of Biostatistics, Vanderbilt University, Nashville, Tennessee 37232

Jennifer G. Whisenant and Richard G. Abramson
Institute of Imaging Science, Vanderbilt University, Nashville, Tennessee 37232 and Department of Radiology and Radiological Sciences, Vanderbilt University, Nashville, Tennessee 37232

Hannah M. Linden
Department of Medical Oncology, University of Washington, Seattle, Washington 98195

Paul E. Kinahan
Department of Radiology, University of Washington, Seattle, Washington 98195; Department of Bioengineering, University of Washington, Seattle, Washington 98195; Department of Physics, University of Washington, Seattle, Washington 98195; and Department of Electrical Engineering, University of Washington, Seattle, Washington 98195

Thomas E. Yankeelov[a)]
Institute of Imaging Science, Vanderbilt University, Nashville, Tennessee 37232; Department of Radiology and Radiological Sciences, Vanderbilt University, Nashville, Tennessee 37232; Department of Biomedical Engineering, Vanderbilt University, Nashville, Tennessee 37232; Department of Physics, Vanderbilt University, Nashville, Tennessee 37232; and Department of Cancer Biology, Vanderbilt University, Nashville, Tennessee 37232

(Received 22 August 2014; revised 6 May 2015; accepted for publication 7 May 2015; published 9 June 2015)

Purpose: Previous studies have demonstrated how imaging of the breast with patients lying prone using a supportive positioning device markedly facilitates longitudinal and/or multimodal image registration. In this contribution, the authors' primary objective was to determine if there are differences in the standardized uptake value (SUV) derived from [^{18}F]fluorodeoxyglucose (18F-FDG) positron emission tomography (PET) in breast tumors imaged in the standard supine position and in the prone position using a specialized positioning device.
Methods: A custom positioning device was constructed to allow for breast scanning in the prone position. Rigid and nonrigid phantom studies evaluated differences in prone and supine PET. Clinical studies comprised 18F-FDG-PET of 34 patients with locally advanced breast cancer imaged in the prone position (with the custom support) followed by imaging in the supine position (without the support). Mean and maximum values (SUV_{peak} and SUV_{max}, respectively) were obtained from tumor regions-of-interest for both positions. Prone and supine SUV were linearly corrected to account for the differences in 18F-FDG uptake time. Correlation, Bland–Altman, and nonparametric analyses were performed on uptake time-corrected and uncorrected data.
Results: SUV from the rigid PET breast phantom imaged in the prone position with the support device was 1.9% lower than without the support device. In the nonrigid PET breast phantom, prone SUV with the support device was 5.0% lower than supine SUV without the support device. In patients, the median (range) difference in uptake time between prone and supine scans was 16.4 min (13.4–30.9 min), which was significantly—but not completely—reduced by the linear correction method. SUV_{peak} and SUV_{max} from prone versus supine scans were highly correlated, with concordance correlation coefficients of 0.91 and 0.90, respectively. Prone SUV_{peak} and SUV_{max} were significantly lower than supine in both original and uptake time-adjusted data across a range of index times ($P << 0.0001$, Wilcoxon signed rank test). Before correcting for uptake time differences,

Bland–Altman analyses revealed proportional bias between prone and supine measurements (SUV_{peak} and SUV_{max}) that increased with higher levels of FDG uptake. After uptake time correction, this bias was significantly reduced ($P < 0.01$). Significant prone-supine differences, with regard to the spatial distribution of lesions relative to isocenter, were observed between the two scan positions, but this was poorly correlated with the residual (uptake time-corrected) prone-supine SUV_{peak} difference ($P = 0.78$).

Conclusions: Quantitative 18F-FDG-PET/CT of the breast in the prone position is not deleteriously affected by the support device but yields SUV that is consistently lower than those obtained in the standard supine position. SUV differences between scans arising from FDG uptake time differences can be substantially reduced, but not removed entirely, with the current correction method. SUV from the two scan orientations is quantitatively different and should not be assumed equivalent or interchangeable within the same subject. These findings have clinical relevance in that they underscore the importance of patient positioning while scanning as a clinical variable that must be accounted for with longitudinal PET measurement, for example, in the assessment of treatment response.
 [http://dx.doi.org/10.1118/1.4921363]

Key words: FDG PET, breast cancer, phantom, positron emission tomography, patient positioning, prone, supine

1. INTRODUCTION

Virtually, all [^{18}F]fluorodeoxyglucose (18F-FDG) positron emission tomography (PET) examinations of the breast in the clinic today are performed with the patient lying in the supine position. However, emerging evidence suggests 18F-FDG-PET in the prone position may offer advantages when compared to the conventional supine position. Prone imaging with breasts hanging pendant allows for improved separation of breast tissue from the myocardium and liver, which helps reduce scatter into these organs, as well as reducing artifacts due to respiratory and other motion during scanning. Detection and classification of breast cancer lesions are potentially improved with prone imaging relative to conventional supine imaging.[1–5] Compared to supine, prone 18F-FDG-PET/CT provides statistically identical information on anatomical disease distribution in locally advanced breast cancer (LABC), with prone scanning performing better than supine at determining the number of involved lymph nodes.[6]

In order to integrate information from different imaging modalities and/or to serially assess FDG-PET data from breast tissue at the voxel level, one must be able to spatially coregister the data obtained at each imaging session, a goal that is greatly facilitated by imaging the breast while patients lay in the prone position on a supportive device.[4,5,7,8] Quantitative evaluation of PET images to assess response to therapy should account for confounding effects. Two of the largest sources of variation are the amount of injected 18F-FDG and the size of the patient. To approximately normalize for these two effects, the standardized uptake value (SUV) is a measure of uptake defined as the tissue activity per unit volume normalized by the decay-corrected injected activity and body weight. The advantage of the SUV metric is the ability to compare uptake intensities between patient images. The most common approach is to normalize activity concentration to patient body weight or lean-body-mass.[9]

There are currently limited data comparing SUV measurements of prone and supine PET imaging of the breast. Direct comparison of data acquired in the two orientations within the same subject following an injection of 18F-FDG is technically challenging as the two scans must necessarily be separated in time. However, the uptake of 18F-FDG is a dynamic, time-dependent process, typically with linearly increasing uptake of 18F-FDG from roughly 25–75 min,[10] which is not accounted for by the SUV calculation.

For quantitative 18F-FDG-PET imaging, consensus recommendations are that the uptake time ranges between 55 and 75 min.[11] Consistently achieving this uptake time in a clinical practice is not always feasible, leading to considerable variability in this parameter across studies. This has high clinical relevance in oncology, particularly when comparing PET data from different institutions or assessing follow-up scans after the initiation of therapy.[12] Methods for modifying PET data to account for differences in 18F-FDG uptake time have been proposed.[10,13–16] A straightforward method for comparing uptake values acquired at different times after injection was introduced by Beaulieu and colleagues.[10] Importantly, this method was developed and prospectively validated in a breast cancer patient population. The Beaulieu method demonstrated low error rates over a wide range of SUVs, which exhibited linear behavior over a range of 18F-FDG uptake intervals similar to the present study. Recently, this approach was demonstrated in liver metastases from colorectal cancer.[16]

Working in LABC patients, we acquired static 18F-FDG-PET images in the prone and then supine positions and investigated the relationship between SUV data acquired in 18F-FDG-PET scans obtained in these two positions. We also characterized the attenuation properties of the prone support structure and differential artifacts within the prone and supine positions, as well as examined the method of accounting for within-patient differences in 18F-FDG uptake time. We tested the hypothesis that prone and supine 18F-FDG-PET scans, when properly corrected for uptake time, result in statistically indistinguishable SUVs.

2. METHODS AND MATERIALS

2.A. Prone support device

Imaging of breast cancer patients in the prone position was conducted using a custom-built torso support device.[7] This device (Fig. 1) is a geometric replica of a double-breast radiofrequency coil apparatus for 3 T MRI (Philips Achieva, Philips Healthcare, Best, The Netherlands). The semirigid torso support is constructed from polystyrene foam insulation (McMaster, Atlanta, GA) and lined with commercially available padding, allowing the breasts to lay pendant with minimal discomfort and consistent positioning. The device was designed with low atomic number materials to minimize attenuation effects.

2.B. X-ray CT and 18F-FDG-PET characterization of the prone support device

To characterize the quantitative impact of the prone support device on 18F-FDG-PET/CT imaging, we first imaged a breast phantom positioned with the prone support device and again without the device and then compared the image quality and quantitative recovery of tracer concentration between the two scans [Fig. 1(A)]. The phantom was a rigid breast attachment to a torso phantom (model ECT/FIL-BR/P, Data Spectrum Corp., Durham, NC); the torso portion of the phantom was not used. Figure 1(A) shows the prone support device (top) and the phantom positioning with (bottom left) and without (bottom right) the device prior to entry into the PET/CT scanner (Discovery STE PET, 16-slice Lightspeed CT, GE Healthcare, Waukesha, WI). The phantom was filled with water (0.98-1 L); each side contained 3.0 kBq/ml of 18F-FDG. PET/CT acquisition and reconstruction parameters were identical to those used in our clinical protocol (see below).

Images of the phantom with and without the prone support device were compared qualitatively and quantitatively. For the qualitative evaluation, we examined the data for image artifacts that may have resulted from 511 keV photon attenuation or scatter due to the positioner that was not properly corrected by standard data correction and processing methods. For the quantitative evaluation, we compared the known 18F-FDG activity concentration within the phantom to activity concentrations measured with and without the prone support device compared to the known true activity. The mean activity concentration was measured in the breast by drawing 11.8 cm^2 elliptical regions of interest (ROIs) in each lobe and calculating the mean value; ROI means were then averaged over 15 image slices.

A second set of phantom experiments were performed to quantify differences in attenuation and scatter between prone versus supine photon sources [Fig. 1(B)]. To simulate an approximate dose of 370 MBq for a 70 kg patient, 3.63 kBq/ml 18F-FDG was prepared within a NEMA IQ body phantom, to which two I.V. bags (0.5 and 1 L, to simulate the breasts) injected with 1.81 kBq/ml 18F-FDG were attached. For the prone PET and CT scans, the body phantom was positioned with the bags hanging pendant and placed within the supportive device [Fig. 1(B), left and top right]. For the supine PET and CT scans, the bags were taped in place adjacent to the anterior wall of the body phantom [Fig. 1(B), bottom right]. A separate clinical CT scan (120 kVp, 375 mA, 0.8 s rotation, and pitch 1.375) was performed after each PET scan, which was acquired in 3D mode for 10 min/bed position and reconstructed using the scanner's built-in ordered subsets expectation maximization (28 subsets, 4 iterations, and 8 mm

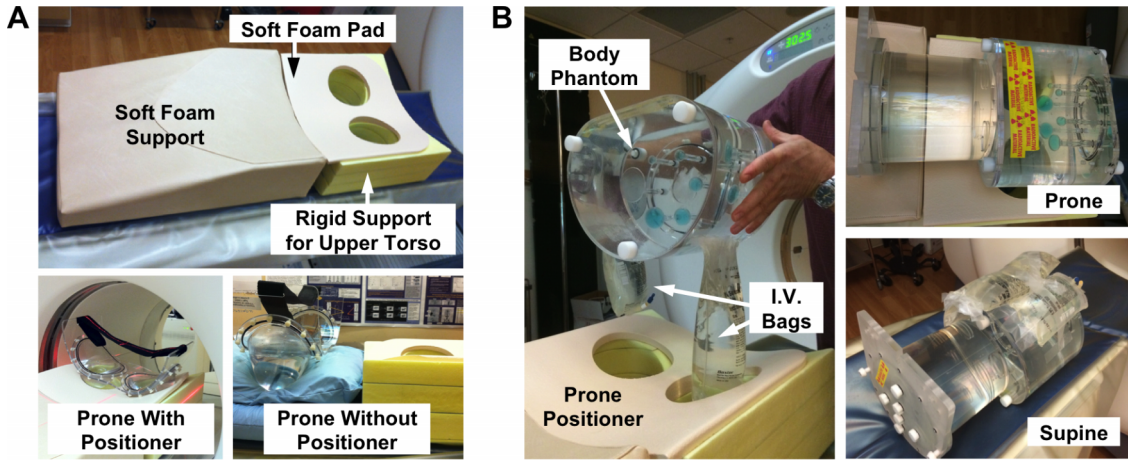

FIG. 1. Apparatuses for phantom experiments evaluating prone and supine PET/CT. (A) First, a rigid phantom study characterized effects of prone support device on lesion detection. Top, prototype prone positioner for PET and MR imaging of breast consists of a soft foam support ramp, a rigid foam upper torso support with breast cutouts covered with a soft foam pad. Bottom left, breast phantom prone in the positioning device, in the CT field of view. Bottom right, phantom without the positioning device. The prone positioning device is seen on the right side for comparison of relative phantom height with and without the device; the prone positioner was removed from the scanner bed for the without-positioner scan. (B) Second, a nonrigid phantom study evaluated position-dependent differences in attenuation between prone and supine images. Left, positioning of body phantom with affixed intravenous (I.V.) saline bags (mock breasts) containing 18F-FDG hanging pendant prior to placement in the scanner. Top right, for prone scans, I.V. bags were positioned inside the prone positioner cutouts and the body phantom was placed on top of the torso support. Bottom right, for supine scans, the positioner was removed and I.V. bags were taped adjacent to the anterior wall of the body phantom.

smoothing), yielding a reconstructed PET image having a slice thickness of 3.27 mm, a 128×128 transaxial matrix, and a 5.47 mm^2 pixel spacing. The mean activity concentration was measured by drawing a 4×4×4 cm ROI over 12 slices on the body phantom and a 2×2×2 cm ROI over 6 slices on the 1-L I.V. bag. Activities were decay-corrected back to the acquisition time of the first scan.

2.C. Clinical 18F-FDG-PET data acquisition

2.C.1. Patient population

For comparison of prone versus supine PET imaging, we imaged 34 patients who were diagnosed with measurable, histologically proven, locally advanced breast cancer and who were scheduled to undergo neoadjuvant chemotherapy in a prospective, longitudinal imaging study (ClinicalTrials.gov identifier NCT01222416). 18F-FDG-PET/CT was performed at three visits in this study: prior to the start of neoadjuvant chemotherapy (baseline), after one cycle, and after completion of therapy. While no patients were excluded or withdrew from the study for any reason, this report describes analyses of the baseline PET data only. Informed consent was obtained for all patients prior to each scanning visit. All aspects of this study were reviewed and approved by local Institutional Review Boards.

2.C.2. Patient preparation

Patients were instructed to fast at least six hours before PET imaging. Blood glucose was measured prior to 18F-FDG injection and verified not to exceed the institutional limit of 200 mg/dl. Approximately 5.8 MBq/kg of 18F-FDG (median 429 MBq; range 291–569) was then administered via the antecubital vein contralateral to the affected breast. Patients were then instructed to lie still in a dimmed room and refrain from physical activity prior to scanning (~60 min). Before positioning on the imaging table, patients were instructed to void the bladder.

2.C.3. PET/CT data acquisition and reconstruction

Clinical PET images were acquired on a Discovery STE scanner (GE Healthcare, Waukesha, WI). For optimal imaging of the breast axillary nodes, prone and supine scans were each performed with the arms elevated above the head. The prone PET scan consisted of 94 slices acquired using the breast support device over two bed positions, resulting in a 3D volume of 83 contiguous slices from the bottom of the skull to the midabdomen. Immediately after completion of the prone scan, the breast support device was removed. A supine PET scan consisting of 376 slices was acquired over eight bed positions, resulting in a 3D volume of 299 contiguous slices from the top of the skull to midthigh. Both PET scans were acquired in 3D mode with 47 slices (2 min) per bed position, each overlapped by 11 slices. With each PET scan, a CT scan was acquired for attenuation correction (AC) and anatomical localization (120 kVp, 80 mA, 0.8 s rotation, and pitch 1.675). PET images were reconstructed using the scanner's iterative mode (20 subsets, 2 iterations, and 6 mm smoothing) with all corrections applied. The reconstructed PET image used a 3.27 mm slice thickness and a 128×128 transaxial matrix with a 5.47 mm^2 pixel spacing.

2.C.4. Quantification of 18F-FDG uptake in patients with locally advanced breast cancer

18F-FDG-PET/CT data were analyzed according to standard methods.[9,17,18] Specifically, for semiquantitative determination of tissue 18F-FDG uptake, PET image values in Bq/ml were converted to SUV via an in-house MATLAB v.R2010b (Mathworks, Natick, MA) script, in a voxelwise manner, as follows: $SUV = A/(I'/W)$, where A is the activity concentration in the PET image (Bq/ml), I' is the decay-corrected injected activity (Bq), and W is the patient body weight (g). Target lesions were identified and outlined according to region-of-interest methodology described in PET response criteria in solid tumors[9] (PERCIST) using algorithms developed in MATLAB. Two standard PET metrics were examined: the maximum SUV of an individual tumor voxel (SUV_{max}) and the mean value of a 1 cm^3 sphere (SUV_{peak}) that included SUV_{max}. Visualization and fusion of 3D PET and CT images were performed in OsiriX (OsiriX Foundation, Geneva, Switzerland). All PET data were anonymized and uploaded to The Cancer Imaging Archive.[19]

2.C.5. Correction of differences in 18F-FDG uptake time

Beaulieu *et al.*[10] described a method to account for differences in 18F-FDG uptake times between scans and showed that the change in SUV over time was approximately linear 27–75 min following 18F-FDG injection (see Fig. 1 in Ref. 10). This allows one to perform linear regression on each time activity curve to estimate intercept and slope constants (a and b, respectively) required to estimate the SUV at a desired index time (t_i). The current study utilizes only two time points (i.e., prone and supine scans) for each patient. Thus, we cannot perform linear regression to estimate the slopes needed to directly obtain a and b. However, the Beaulieu *et al.* method was conducted in patients with locally advanced breast cancer under very similar experimental conditions as our patient data, making the application of slopes obtained in their study appropriate for estimating a and b in the current study. Once these two parameters are determined using the assumed slope, extrapolation of SUVs for prone and supine data to a common t_i makes the two scans comparable. The clinical target t_i of 60 min was chosen to compare uptake time-adjusted prone and supine PET/CT data (referred to throughout this report as SUV_{peak}' and SUV_{max}'). Additional analyses compared prone and supine data using other t_i's (45, 75, and 90 min) that approximated the range of uptake times in our patient data (54.4–92.4 min). All uptake time-corrected data were derived using slope ($SUV_{peak} = 0.010$, $SUV_{max} = 0.011$) and intercept ($SUV_{peak} = -0.026$, $SUV_{max} = -0.033$) parameters determined at the 71–75 min reference time (see Table I in

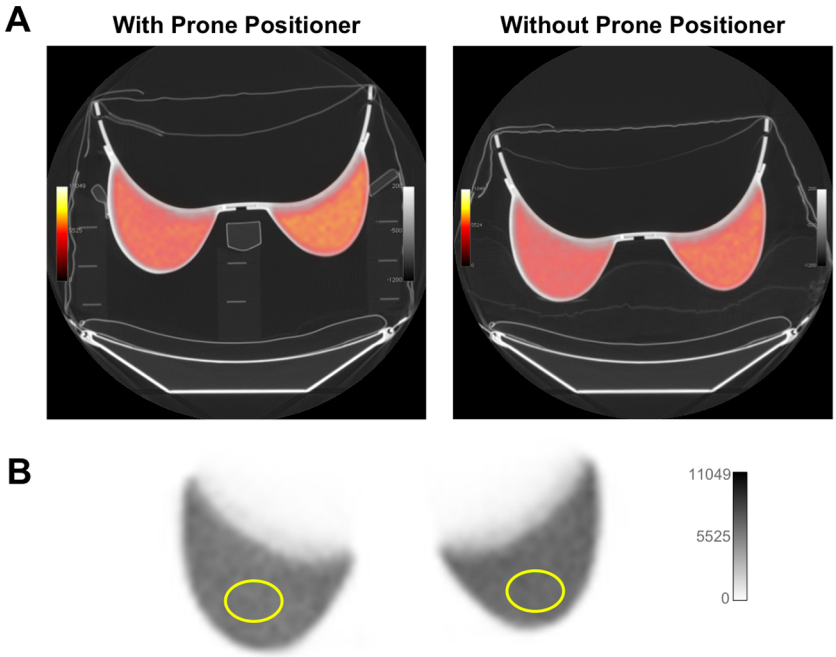

FIG. 2. Characterization of prone positioner with rigid breast phantom. (A) PET/CT of breast phantom with (left) and without (right) the prone positioner. PET images were fused with CT scans set to a pulmonary gray scale level for visualization of low-density materials of the positioner and pillow support in the scan without positioner. PET images were scaled to compensate for the activity decay between scans (22 min). (B) Elliptical ROIs (11.8 cm^2) were drawn over each side of the phantom to measure activity concentration. Values in Table I represent the average of 15 ROI means (from one side of the phantom) over 15 image slices.

Ref. 10), where estimated SUVs were best correlated with actual SUVs.

2.D. Statistical analysis of clinical data

Data were analyzed using R Statistical Software v.3.0 (www.r-project.org). For all statistical tests, the level of significance was set at $\alpha = 0.05$. Analyses involving multiple statistical tests were corrected using the Bonferroni method at familywise Type I error of 0.05. The Wilcoxon matched-pairs signed rank test was used to examine within-subject differences between prone and supine SUV_{peak} or SUV_{max}. The same nonparametric tests were used to examine the effects of linearly correcting for differences in 18F-FDG uptake time (as described above) on (1) each measure (SUV_{peak} or SUV_{max}) acquired in a specific position (prone or supine) and (2) the difference in each measure between the acquisition positions. Kruskal–Wallis, linear regression, and Pearson correlation analyses were conducted in Prism v.5.0f (GraphPad Software, Inc., La Jolla, CA) to evaluate the precision of the correlation and test for significant differences among subgroups. The concordance correlation coefficient (CCC) was computed in MATLAB to determine accuracy of correlation between variables.[20] The Bland–Altman method was used to visually inspect the agreement in SUV_{peak} and SUV_{max} between prone and supine positions. The null hypothesis is that there is no significant difference between lesion SUV_{peak} or SUV_{max} obtained in the prone versus supine position.

3. RESULTS

3.A. Characterization of prone and supine 18F-FDG-PET/CT with breast phantoms

We first examined the effects of the prone positioning device itself on PET and CT images, using a breast phantom with and without the prone positioner as shown in Fig. 2. Visual assessment did not reveal any difference in subjective appearance between the two PET images. The mean SUV in the rigid breast phantom placed on the positioner was 1.92% lower than the mean SUV determined when the positioner was removed (Table I). Results shown in the table reflect

TABLE I. Activity concentrations measured in the breast phantom within the prone positioner (kBq/ml).

	True activity	Measured activity (mean ± SD)	CoV[a] (%)	Percent activity error[b] (%)	SUV[c]
With positioner	3.37	3.43 ± 0.15	4.37	1.75	1.02
Without positioner	2.95	3.08 ± 0.042	1.36	4.22	1.04

[a]CoV, coefficient of variation, i.e., image noise = SD/mean.
[b]Percent activity error, i.e., recovery = (measured − true)/measured.
[c]SUV, standardized uptake value = measured/true.

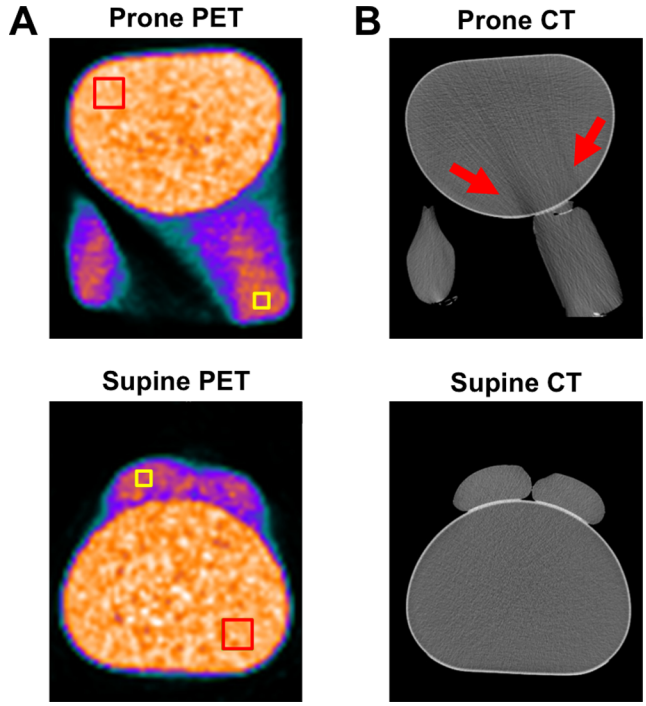

FIG. 3. Characterization of differences in attenuation between prone (top) and supine (bottom) PET scans. (A) ROIs were drawn on PET images over a distal portion of the 1-l I.V. bag and the contralateral posterior quadrant of the body phantom (squares). (B) CT images of phantom in the prone position showed a streaking artifact (arrows), which was not observed in the supine scan. The results of the ROI analyses are shown in Table II.

values from one side of the phantom; nearly identical values were obtained from the other side (data not shown).

We next sought to characterize differences in attenuation and scatter correction between prone and supine 18F-FDG-PET/CT images (Fig. 3). To do this, mock breasts (I.V. bags filled with 18F-FDG) were attached to a standard body phantom and imaged in the prone position within the support device [Fig. 3(A), top], or they were imaged in the supine position without the device but with the bags affixed to the anterior wall of the body phantom [Fig. 3(A), bottom]. The ROIs on PET images in Fig. 3(A) were positioned over the I.V. bags and the body phantom and quantified in Table II. CT scans are shown in Fig. 3(B) and indicated a streaking artifact in the anterior chest wall portion of the body phantom emanating from the support cutout containing the 1-l I.V. bag mock breast. Although prone PET images were free of this streaking artifact, the reduction in central Hounsfield units in CT images led to a reduction in central PET SUV.

3.B. Prone and supine 18F-FDG-PET/CT imaging in breast cancer patients

Table III summarizes the demographics and baseline disease characteristics of the patients. The majority had clinical stage II or stage IIIA disease, with high-grade tumors averaging 5.1 cm in diameter (range 1–10 cm). Approximately, half of the patients had axillary node involvement, and nearly one-third had triple negative LABC. Primary tumors affected only one breast in all but one patient (P24), whose bilateral tumors were analyzed independently, i.e., a total of 35 primary lesions underwent ROI analyses. Detailed characteristics for each patient are listed in Table I of the supplementary material.[22]

To correct for differences in FDG uptake time between the prone and supine PET scans, we applied the method of Beaulieu *et al.*[10] Figure 4 illustrates the range of 18F-FDG uptake times and SUV_{peak} [Figs. 4(A) and 4(B)] and SUV_{max} [Figs. 4(C) and 4(D)]. Before correcting for uptake time, the median (range) prone and supine SUV_{peak} were 7.60 (1.60–20.5) and 8.99 (1.73–22.7), respectively; the median (range) prone and supine SUV_{max} were 9.28 (1.90–21.7) and 11.4 (2.09–26.1). SUV_{peak} and SUV_{max} from prone versus supine PET were well correlated, with CCC of 0.912 and 0.900, respectively. Consistent with trends observed in Beaulieu *et al.*,[10] the simple difference in SUV_{peak} or SUV_{max} between prone and supine scans was proportional to the magnitude of these measurements: prone PCC (95%CI) = 0.612 (0.350–0.785), $P < 0.0001$; supine PCC (95%CI) = 0.723 (0.513–0.851), $P < 0.0001$.

Table IV summarizes the median and range of SUV_{peak} and SUV_{max} values for prone and supine positions. For both SUV_{peak} and SUV_{max}, significant differences between prone and supine data were observed, both before and after adjusting SUV to a common index time. For corrected data, these statistically significant differences were observed at each of four index times ($t_i = 45$, 60, 75, and 90 min), which

TABLE II. Comparison of prone and supine mean activity concentrations measured in nonrigid breast and rigid body phantoms (kBq/ml). Prone/supine activity values were decay-adjusted to the start time of the first acquisition to compensate for time between scans.

Scan object	Scan position	True activity	Measured activity (mean ± SD)	CoV[a] (%)	Percent activity error[b] (%)	SUV[c]
Body phantom	Prone	3.40	3.15 ± 0.13	4.13	−7.94	0.93
	Supine		3.16 ± 0.14	4.43	−7.59	0.93
1-l I.V. bag	Prone	1.79	1.76 ± 0.06	3.41	−1.70	0.98
	Supine		1.85 ± 0.10	5.41	3.24	1.03

[a]CoV, coefficient of variation, i.e., image noise = SD/mean.
[b]Percent activity error, i.e., recovery = (measured − true)/measured.
[c]SUV, standardized uptake value = measured/true.

TABLE III. Summary patient demography and disease characteristics ($n = 34$ patients).

Variable (units)	Number, median (range, %)
Age (yr)	48 (31–67)
Body mass (kg)	76 (45–105)
Height (m)	1.65 (1.52–1.75)
Lean body mass (kg)	48.7 (36.0–55.9)
Race	
African-American	10 (29%)
Caucasian	24 (71%)
Ethnicity	
Hispanic	1 (3%)
Non-Hispanic	33 (97%)
Affected breast	
Right only	20 (59%)
Left only	13 (38%)
Bilateral	1 (3%)
TNM clinical stage	
Stage I	1 (3%)
Stage IIA/IIB	6 (18%)/7 (21%)
Stage IIIA/IIIB/IIIC	12 (35%)/2 (6%)/1 (3%)
Stage IV (metastatic)	2 (6%)
N/A	3 (9%)
Tumor diameter	5.0 cm (1.0–10.0 cm)
Clinical node status	
Positive	19 (56%)
Negative	9 (26%)
N/A	6 (18%)
Tumor grade	
Low	1 (3%)
Intermediate	7 (21%)
High	24 (71%)
N/A	2 (6%)
Hormone receptor status	
ER (+/−/N/A)	14 (41%)/19 (56%)/1 (3%)
PR (+/−/N/A)	10 (29%)/23 (68%)/1 (3%)
HER2 (+/−/equivocal)	13 (38%)/19 (56%)/1 (3%)
Triple negative (ER-, PR-, HER2-)	11 (32%)

Note: TNM = tumor-node-metastasis staging system; ER = estrogen receptor; PR = progesterone receptor; HER2 = human epidermal growth factor receptor 2; N/A = not available.

spanned the range of uptake times from the original prone and supine scans. Original and corrected ($t_i = 60$ min) data from each patient are listed in Table II of the supplementary material.[22]

We next applied the Bland–Altman method to evaluate the agreement and reproducibility of SUV_{peak} and SUV_{max} measurements obtained from prone versus supine PET (Fig. 5). Among the four PET metrics of interest, there was no statistically significant difference observed in the bias estimates (mean prone-supine difference, solid lines, with 95% confidence intervals, dashed lines): −1.71 (−4.36 to 0.94) for SUV_{peak} [Fig. 5(A)], −0.82 (−2.49 to 0.86) for SUV_{peak}' [Fig. 5(B)], −2.08 (−5.13 to 0.97) for SUV_{max} [Fig. 5(C)], and −0.86 (−2.67 to 0.96) for SUV_{max}' [Fig. 5(D)]; $P = 0.3916$ (Kruskal–Wallis test). Inspection of the two plots before correction of uptake time differences [Figs. 5(A) and 5(C)] indicated proportional bias, confirmed by statistically significant deviation from zero of the slope (difference versus average) estimates ($SUV_{peak} F_{1,33} = 44.4$, $P < 0.0001$; $SUV_{max} F_{1,33} = 45.7$, $P < 0.0001$). After correcting for the uptake time differences, proportional bias was significantly reduced ($SUV_{peak}' F_{1,33} = 5.26$, $P = 0.0283$; $SUV_{max}' F_{1,33} = 3.47$, $P = 0.0713$), and good agreement between prone and supine data was achieved [Figs. 5(B) and 5(D)].

The potential exists for differential spatial resolution, as a function of lesion geometric positioning within the PET scanner's field-of-view (FOV), to play a role in the residual (i.e., uptake time-corrected to $t_i = 60$) prone-supine SUV_{peak}' difference we observed. Figure 6 illustrates the 2D distribution of lesions with respect to the FOV center in the transverse (TV) and axial (Z) planes in prone and supine PET [Figs. 6(A) and 6(D), respectively]. Statistically significant differences were observed between prone and supine lesion-to-FOV center distance in the transverse [Fig. 6(B)] and axial [Fig. 6(E)] planes ($P < 0.0001$, Wilcoxon signed rank test). Analysis of lesion distance to TV FOV center with SUV_{peak}' yielded a statistically significant correlation for both scanning positions: prone PCC = −0.42, $r^2 = 0.18$, $P = 0.0122$; supine PCC = −0.48, $r^2 = 0.23$, $P = 0.0039$. In contrast, correlation of lesion distance to axial FOV center with SUV_{peak}' was not statistically significant for either position: prone PCC = 0.17, $r^2 = 0.027$, $P = 0.344$; supine PCC = 0.13, $r^2 = 0.017$, $P = 0.463$. Differences in SUV_{peak}' from prone and supine scans were compared pairwise to their corresponding differences in lesion distance to FOV center in the TV and axial planes. Because PET spatial resolution decreases nonlinearly with respect to the TV FOV center, the prone-supine difference in each lesion was normalized to the prone value. In either plane, the correlation was not statistically significant: transverse PCC = −0.049, $r^2 = 0.0024$, $P = 0.778$ [Fig. 6(C)]; axial PCC = 0.011, $r^2 = 0.000\,13$, $P = 0.95$ [Fig. 6(F)].

The percentage error observed with the Beaulieu *et al.*[10] correction method applied to SUV_{peak} correlated well with uptake time for both scan positions: prone PCC (95%CI) = 0.801 (0.638–0.895), $P < 0.0001$; supine PCC (95%CI) = 0.845 (0.712–0.919), $P < 0.0001$. This correlation was also observed with SUV_{max}: prone PCC (95%CI) = 0.783 (0.608–0.885), $P < 0.0001$; supine PCC (95%CI) = 0.838 (0.700–0.916), $P < 0.0001$. Original SUV_{peak} versus SUV_{max} values were well correlated for both scan orientations: prone PCC = 0.987, CCC = 0.915; supine PCC = 0.989, CCC = 0.918. Uptake time-corrected SUV_{peak} versus SUV_{max} values were likewise correlated: prone PCC = 0.986, CCC = 0.684; supine PCC = 0.987, CCC = 0.686. Analyses of these correlations with regard to prone-supine differences resulted in the following: original values PCC = 0.905, CCC = 0.869; uptake time-corrected values PCC = 0.790, CCC = 0.786.

Figure 7 depicts representative 3D 18F-FDG-PET/CT images displayed in axial, coronal, and sagittal planes from three patients that illustrate the range of prone-supine SUV_{peak} differences observed in the clinical study. The patient in Fig. 7(A) had a multifocal primary tumor (arrows) that achieved qualitatively better separation from two FDG-avid axillary

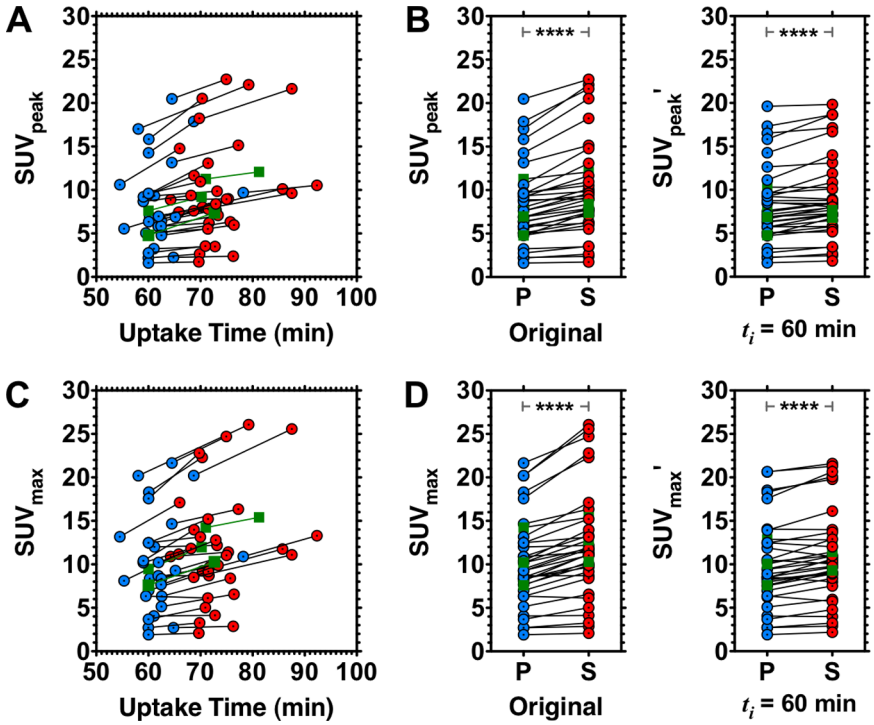

FIG. 4. SUV_{peak} and SUV_{max} as a function of 18F-FDG uptake time. Original SUV_{peak} [(A); (B), left panel] and SUV_{max} [(C); (D), left panel] and uptake time-adjusted ($t_i = 60$ min) SUV_{peak}' [(B), right panel] and SUV_{max}' [(D), right panel). Circles indicate values from prone PET (P); adjoining circles indicate values from supine PET (S). Squares represent example subjects illustrated in Fig. 7. ****$P << 0.0001$, Bonferroni-corrected Wilcoxon signed rank test.

nodes (arrows) in the prone position compared to supine. This patient had a mean prone-supine percentage difference in SUV_{peak} that very closely approximated the mean difference for the entire group (11% after uptake time-adjustment). Figure 7(B) shows another patient with a small unifocal tumor of the right breast who exhibited the largest prone-supine percentage difference in SUV_{peak} for the group (35% after uptake time-adjustment). Finally, in Figs. 7(C) and 7(A),

TABLE IV. Effects of adjusting SUV for uptake time ($n = 35$ lesions).

	Prone, median (range)	Supine, median (range)	P vs S median, P value[a]	Prone error[b], median (range)	Supine error[b], median (range)	P vs S error, P value[a]
			SUV_{peak}			
Original value	7.60 (1.60–20.5)	8.99 (1.73–22.7)	1.24×10^{-06}	n/a	n/a	n/a
Corrected value[c]						
$t_i = 45$ min	6.39 (1.77–16.8)	7.11 (1.95–16.9)	1.78×10^{-05}	11.3 (0.97–22.7)	18.2 (0.42–32.1)	1.40×10^{-06}
$t_i = 60$ min	7.16 (1.60–19.6)	8.03 (1.82–19.8)	1.78×10^{-05}	1.14 (0.00–12.4)	8.26 (0.00–20.8)	2.16×10^{-06}
$t_i = 75$ min	7.92 (1.43–22.5)	8.94 (1.68–22.7)	1.78×10^{-05}	8.49 (0.97–18.5)	2.16 (0.02–10.8)	6.60×10^{-05}
$t_i = 90$ min	8.69 (1.27–25.4)	9.86 (1.55–25.6)	1.78×10^{-05}	19.3 (1.94–32.1)	10.3 (0.34–20.8)	1.29×10^{-06}
			SUV_{max}			
Original value	9.28 (1.90–21.7)	11.4 (2.09–26.1)	2.09×10^{-06}	n/a	n/a	n/a
Corrected value[c]						
$t_i = 45$ min	7.79 (2.11–17.3)	8.73 (2.33–18.1)	1.48×10^{-04}	13.5 (1.94–24.5)	21.1 (1.52–34.9)	1.18×10^{-06}
$t_i = 60$ min	8.90 (1.90–20.7)	10.1 (2.18–21.6)	1.48×10^{-04}	1.25 (0.00–13.4)	9.70 (0.79–22.6)	9.91×10^{-07}
$t_i = 75$ min	10.0 (1.69–24.0)	11.4 (2.03–25.1)	1.48×10^{-04}	10.5 (1.31–21.3)	2.45 (0.01–12.0)	6.13×10^{-05}
$t_i = 90$ min	11.1 (1.49–27.3)	12.7 (1.88–28.6)	1.48×10^{-04}	22.1 (3.24–36.9)	12.4 (0.67–23.1)	1.08×10^{-06}

Note: FDG = fluorodeoxyglucose; SUV = standardized uptake value.
[a]Bonferroni-corrected Wilcoxon signed rank test.
[b]Pairwise correction percent error = |original value − corrected value|/original value.
[c]Original prone and supine lesion SUV_{peak} or SUV_{max} were corrected for intersubject differences in FDG uptake time according to the method of Beaulieu *et al.* (Ref. 10) using index times (t_i) encompassing the range of uptake times for the clinical data.

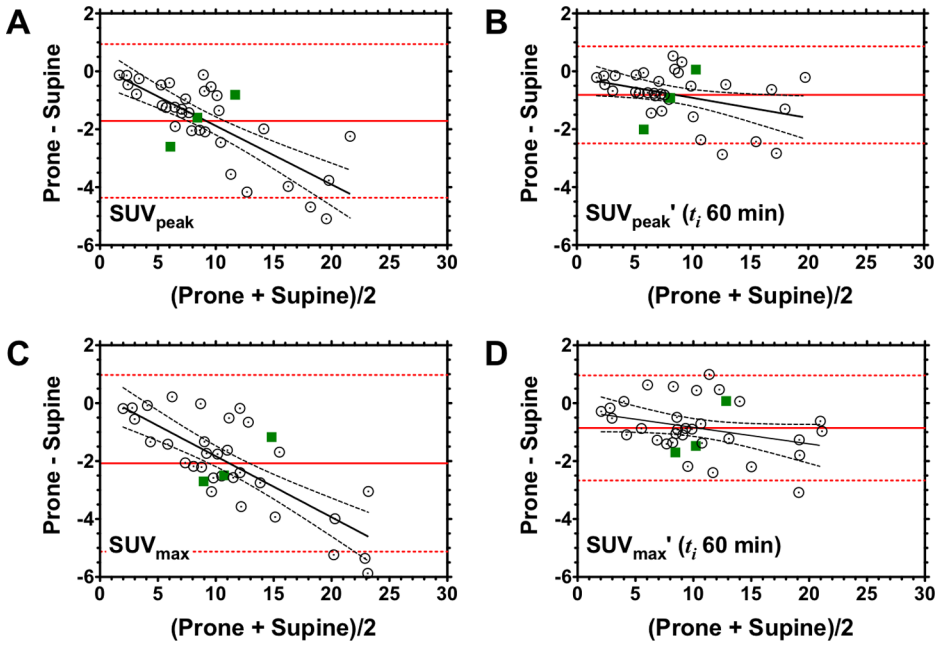

FIG. 5. Agreement between prone and supine measurements of SUV_{peak} and SUV_{max}, before and after correcting for uptake time differences. Original SUV_{peak} (A) and SUV_{max} (C) and uptake time-adjusted ($t_i = 60$ min) SUV_{peak}' (B) of SUV_{max}' (D). Bland–Altman plots for prone and supine data, expressed as the difference between the two positions (prone-supine), are plotted on the abscissa; corresponding mean values (i.e., average of prone and supine) are plotted on the ordinate. Solid horizontal lines represent the mean prone-supine difference. Slope estimates (difference versus mean) were obtained from linear regression. Dashed lines represent the 95% confidence interval. Squares represent example subjects illustrated in Fig. 7.

patient with a medium-sized multifocal tumor had a prone-supine percentage difference in SUV_{peak} that was the smallest for the group (0.2% after uptake time-adjustment).

4. DISCUSSION

4.A. Motivations for the study

Standard clinical FDG PET imaging of the breast is done with the patient lying in the supine position. This makes quantitative lesion evaluation difficult, since in this position the breast flattens, introducing the likelihood for tumor deformation, distortion, and overlap with adjacent anatomy (e.g., axillary nodes). Imaging of the breast in the prone orientation, for instance, with a dedicated support device, ensures that the breast is consistently positioned with repeated scanning, which greatly facilitates longitudinal assessment of tumor response and/or multimodal image coregistration.[4,5,7,8] We have recently completed a preliminary analysis comparing prone and supine PET in the qualitative categorization of the anatomical distribution of disease and in the assessment of the number of involved axillary lymph nodes in LABC patients.[6] As an extension of that effort, the current study was undertaken to quantitatively compare clinically relevant metrics (SUV_{peak}, SUV_{max}) derived from prone versus supine PET. To accomplish this, we first set out to systematically examine the 18F-FDG-PET properties of a dedicated, custom-built prone positioning device in conjunction with phantoms simulating conditions found in prone and supine patient PET/CT scans (Figs. 1–3). We then investigated prone-supine differences in a group of patients diagnosed with LABC using established PET criteria.[9] Because the prone and supine scans were unavoidably separated in time for each subject, it was necessary to apply a correction method[10] to account for differences in 18F-FDG uptake time.

4.B. Summary of phantom studies

We characterized a custom prone positioner used to facilitate longitudinal 18F-FDG-PET imaging with the aim of assessing differences in SUV measured in the prone versus supine positions. Visual assessment of PET and CT scans of the breast phantom with and without the prone positioner showed minimal differences (Fig. 2). Activity concentrations measured in the rigid breast phantom were compared between the images acquired with and without the prone support device. Quantitative assessment (Table I) revealed SUV biases <2%, indicating that the prone positioner does not have any adverse signal attenuating effects on 18F-FDG-PET images. In the nonrigid phantom study, prone CT images contained a streaking artifact in anterior chest areas adjacent to the breast support cups within the positioner [Fig. 3(B)]. Since CT images are used to correct for attenuation in PET images, these streaking artifacts have potential to reduce PET SUV in this body region, although they do not appear in regions in the main phantom outside the artifact region once appropriate decay corrections are applied.

4.C. Summary of clinical study

Statistically significant pairwise differences were observed between SUV_{peak} and SUV_{max} in prone versus supine PET after adjusting the values to the clinical target index time (t_i = 60 min; Fig. 4) and across a range of t_i that encompassed

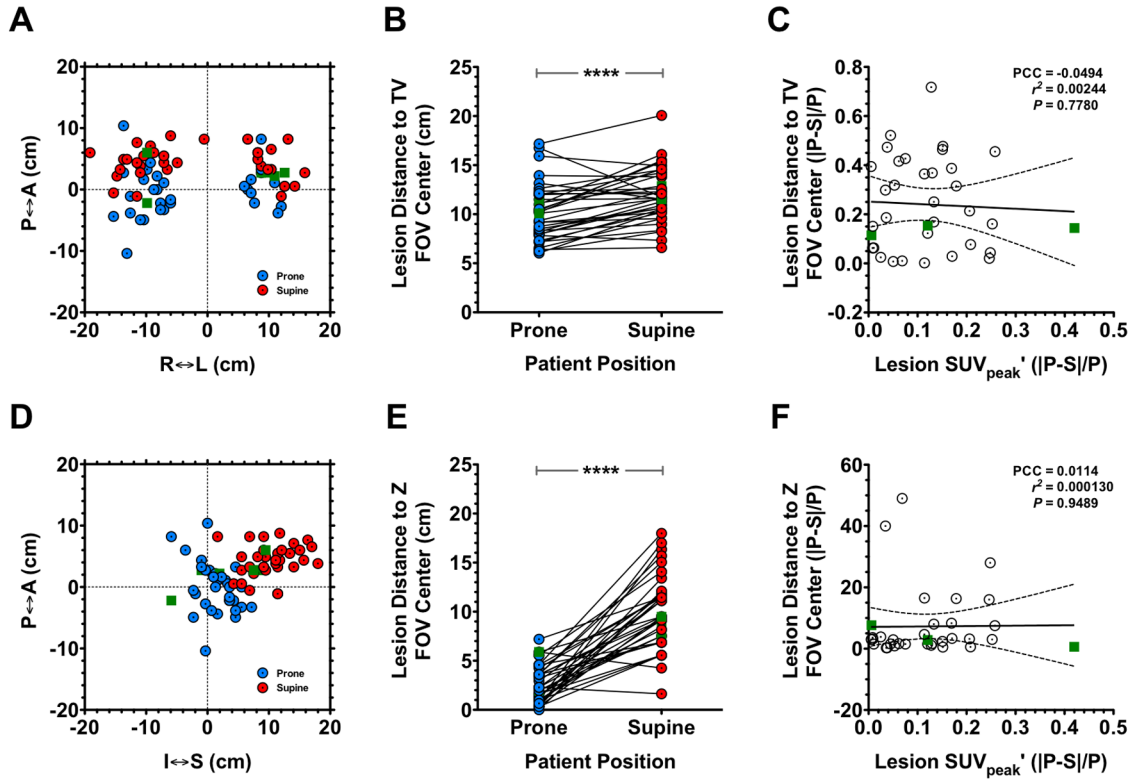

FIG. 6. Relationship between lesion positioning and SUV_{peak} in prone versus supine PET images. [(A) and (D)] Lesion positioning in prone versus supine PET data with respect to transverse [TV; (A)] and axial (Z-axis; D) FOV. [(B) and (E)] Statistical comparisons of prone and supine distance from FOV center. [(C) and (F)] Correlation analyses comparing lesion distance from FOV center versus lesion SUV_{peak}, corrected to $t_i = 60$ min according to Beaulieu *et al.* (Ref. 10). Data are expressed in terms of the absolute difference in prone (P) and supine (S) value in proportion of the prone value ($|P–S|/P$). Squares represent example subjects shown in Fig. 7. $I–S$, inferior–superior; $A–P$, anterior–posterior; $R–L$, right–left. ****$P < 0.0001$, Wilcoxon signed rank test.

the uptake times encountered in the clinical study (Table IV). For both SUV_{peak} and SUV_{max}, we observed good prone-supine agreement using the Bland–Altman approach (Fig. 5), with proportional bias decreasing after correcting uptake time ($t_i = 60$ min). Significant pairwise differences in the geometric displacement from the PET FOV center, both in the transverse plane and along the z-axis, were observed between prone and supine PET. These displacement differences were poorly correlated with corresponding prone-supine differences in SUV_{peak} (Fig. 6). Collectively, these analyses revealed that imaging in the prone position results in SUV_{peak} and SUV_{max} values that are highly correlated with, yet significantly different from, those obtained in the supine position. Furthermore, prone imaging has the added benefit of facilitating and significantly improving longitudinal and/or multimodal image registration (see, e.g., Refs. 7 and 8). Prone 18F-FDG-PET/CT provided qualitatively improved lesion visualization and separation of axillary lymph nodes compared to the supine position [Fig. 7(A); see, e.g., Ref. 6].

4.D. Prior 18F-FDG PET studies evaluating prone-supine differences

While 18F-FDG-PET in the prone position has been shown to improve breast cancer detection[4,5] and facilitate longitudinal coregistration across time points and/or imaging modalities over the course of therapy (see, e.g., Refs. 7 and 8), relatively few studies have directly compared prone and supine 18F-FDG-PET in breast cancer. Yutani *et al.*[2] examined a small number ($n = 18$) of patients and found that prone 18F-FDG-PET resulted in significantly higher SUVs and tumor-to-normal tissue ratios compared to supine. In this study, half of the patients were imaged prone first/supine second while the order was reversed for the other half. Prone imaging resulted in statistically higher SUV in both groups. The mean tumor diameter in that study (1.9 cm; range 0.3–4.2 cm) was considerably lower than the present study (5.1 cm; range 1.0–10 cm), so the comparability of these findings to our own is unclear.

A study by Kaida *et al.*[3] examined differences in prone versus supine 18F-FDG-PET among 118 patients who were suspected of having breast cancer and compared the results of both scans to preoperative histopathological staging results. The authors found significant improvements in detection sensitivity, accuracy, and negative predictive value with prone imaging relative to whole-body supine imaging. The study found a nonsignificant trend toward an increase in SUV_{max} obtained from prone versus supine PET. It is difficult to reconcile these observations with the current study, since the order of the scans in Kaida *et al.* was opposite (i.e., supine first, prone second) of the order used in the current study. Furthermore, the authors used an unpaired Student t-test

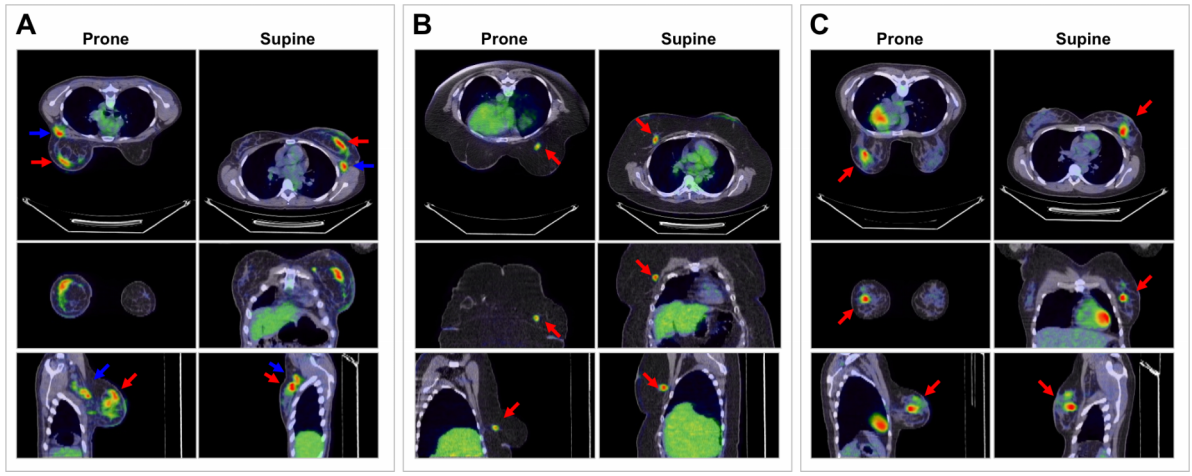

FIG. 7. Fused PET/CT images comparing prone and supine positions. (A) 36-yr old patient (P21) with Stage IIIA, intermediate-grade, node-positive LABC, in whom the prone-supine SUV_{peak} percentage difference ($P–S\%\Delta$), after correcting for uptake time differences ($t_i = 60$ min), closely approximated the corrected group mean $P–S\%\Delta$: P21, 11.4% (0.92 SUV) versus group 11.4% (0.82 SUV). (B) 46-yr old patient (P32) with ER-and HER2-negative, high-grade LABC in whom $P–S\%\Delta$ was the largest in the corrected group: 34.7% (2.01 SUV). (C) 32-yr old patient with ER-/PR-/HER2-positive, high-grade LABC in whom $P–S\%\Delta$ was the smallest in the corrected group: 0.24% (0.018 SUV). Relative to supine position, prone FDG PET/CT with the positioner improved the separation of primary tumor from axilla and chest wall (arrows).

in making their comparisons, in spite of the fact that the measurements being comparing were matched in the same subject. In our study, we observed a small but statistically significant reduction in the prone measurements relative to supine, both before and after uptake time correction across a range of index times (Table IV). We note that in both the Yutani *et al.*[2] and Kaida *et al.*[3] studies, the effect of patient position—specifically as it relates to the basic physics involved with image reconstruction and quantification—was not examined. Combined with the known effect of a trend toward increased SUVs with increased uptake period, quantitative comparison of the results from those studies to the current findings is not straightforward.

The current study adopted the methodology by Beaulieu *et al.*[10] to correct for variation in 18F-FDG uptake times. It should be pointed out that in the above studies—and indeed all of the studies that we have found which pertain to positional effects on SUV quantitation—variability in 18F-FDG uptake time between within-subject scan pairs was not taken into consideration. This is especially important in studies with small sample size, where uptake time variations will influence the magnitude and/or direction of observed prone-supine differences, which collectively have been small in size, when observed at the group level.[13,14]

Finally, to investigate whether the choice of uptake time used in our correction method may have influenced our findings, we compared the uncorrected and the corrected SUV (peak and max) in the prone and supine positions using a range of index times that encompassed those found in the original clinical data. As shown in Table IV, regardless of the choice of index time chosen (45, 60, 75, or 90 min), there are still statistically significant differences in corrected SUV_{peak} and SUV_{max}. We conclude from these data that differences in uptake time alone, or in the choice of index time used to account for those differences, cannot explain the differences in SUV_{peak} and SUV_{max} that we observe.

With the clinical findings suggesting that prone-supine differences in SUV were not the result of different uptake times, or choice of index times, we next examined the potential for differences in the spatial distribution of lesions to play a role. It is known that the spatial resolution of PET varies with radial distance from the FOV center in the transverse plane ($A–P$ by $R–L$). It is likewise appreciated that coincidence efficiency decreases with increasing axial distance from the central slice (i.e., distance from the z-axis FOV center). Interestingly, the current study found significant prone-supine differences in the lesion-to-isocenter offset in both the transverse plane and along the z-axis, but in both cases, there was very poor correlation with the prone-supine differences in SUV_{peak}. Importantly, these observations were made in data corrected to the clinical target index time, $t_i = 60$ min. These findings suggest that, in addition to uptake time, positional differences with respect to lesion positioning relative to the FOV center cannot account for the SUV differences between the two scanning positions.

4.E. Limitations

While the findings from this study are intriguing and potentially of significant clinical relevance, there are some limitations that should be considered. First, the uptake time correction methodology in this study employed the same parameters from Beaulieu *et al.* (see Table I in Ref. 10) since we did not perform dynamic PET imaging to evaluate the intercept and slope. The validity of this method in accounting for differences in uptake time is supported by the similar patient population and disease setting (locally advanced breast cancer) to the present study, enabling us to reasonably apply their parameters to our data. However, given the variability among both patient populations, as well as differences in image acquisition and reconstruction methods between the

two studies, the uptake time correction achieved using the Beaulieu *et al.* approach did not yield statistically equivalent SUVs. It should be noted that the current data were acquired in 3D mode using a GE Discovery STE scanner with CT-based AC and iterative reconstruction, while the Beaulieu *et al.* study was acquired in 2D on an older advance system without CT (pin-source AC) and filtered back projection reconstruction. While the Beaulieu *et al.* linear correction model was based on trends and relative comparisons that in theory would mitigate potential scanner bias, these and other factors do impact SUV derivation and may influence the application of this model to optimally adjust SUV for uptake time differences.

Another potential limitation lies with the current clinical study design, i.e., implementing the same prone-supine scan order in all the patients, rather than a randomized, or at least balanced, scan order. The PET scanners employed in this study have dedicated, institution-specific clinical configurations with established protocols, scheduling, and workflows that limited the logistical feasibility of mixing the scan order among the different patients. Owing to these challenges we used a consistent prone-supine scan order, but corrected for differences in uptake time in a manner that was straightforward and which yielded results that were in good agreement, as indicated by our Bland–Altman analyses (Fig. 5). The Beaulieu *et al.* method was based on approximately linear behavior of SUV within an uptake interval of 27–75 min; however, there were 11 supine scans and 1 prone scan with an uptake time >75 min. Because of this discrepancy and to ensure that the choice of index time was not biasing our results, it was necessary to reexamine the clinical data using multiple index times that spanned the range of the original data. Regardless of the index time chosen, significant differences in corrected prone and supine SUV_{peak} and SUV_{max} were observed, as were differences in pairwise correction error (Table IV). Finally, posthoc statistical analysis of a data subset excluding the 12 patients with uptake times >75 min similarly resulted in significant differences in prone and supine SUVs (data not shown). Collectively, these data suggest that differences in prone and supine scan uptake time resulting from the design of this study cannot account for the SUV differences observed between the two scan positions.[10]

4.F. Future directions

We have found statistically significant residual differences in prone versus supine 18F-FDG-PET/CT metrics (SUV_{peak} and SUV_{max}) in LABC patients prior to the start of neoadjuvant chemotherapy. The clinical significance of these differences remains unclear and warrants further investigation. Recent preliminary analysis of the influence of patient position on the ability of FDG PET to assess response to therapy revealed no appreciable prone-supine difference in predictive utility.[21] Those findings are consistent with the current studies suggesting prone PET—using a support device that itself is resistant to significant adverse affects on image quality—produces results that are highly congruent with (but consistently lower than) supine PET.

5. CONCLUSION

This report is a quantitative extension of our previous study that examined qualitative differences in prone versus supine PET.[6] To our knowledge, the current study is the first to characterize the prone positioner and systematically measure—with assessment of and correction for within-patient uptake time variability—differences, both in terms of two clinically relevant semiquantitative endpoints, SUV_{peak} and SUV_{max}, in 18F-FDG-PET/CT images acquired in the prone versus conventional supine orientations. Prone PET imaging, with the customized torso support device, is now validated for SUV measurements compared to prone imaging without the device. However, phantom studies reveal possible positional differences independent of the support device that could contribute to differences in measured PET values. For small lesions (<2–3 cm diameter) resolution loss, differences in scatter correction, and/or differences in attenuation correction could introduce SUV differences between prone and supine in some cases, so longitudinal scans deployed for therapy response measurement should be consistently done in either the prone or supine orientation. The benefit of scanning in the prone position is that it improves lesion localization allowing longitudinal (and multimodal) comparison. The results of this study may have immediate application to how 18F-FDG-PET data are acquired in the clinical management of patients with primary breast cancer.

ACKNOWLEDGMENTS

Sincerest thanks are offered to the patients and their families for participation in the authors' studies. The authors also thank Dr. Todd Peterson for his thoughtful comments and assistance with this paper. The authors thank the National Cancer Institute for funding through Nos. U01 CA142565, 1U01 CA174706, P50 CA098131, P50 CA138293, and P30 CA68485. J.M.W., S.D.R., X.L., L.R.A., H.K., J.G.W., R.G.A., and T.E.Y. wish to thank the Kleberg Foundation for generous support of the imaging program at their institution.

[a)]Author to whom correspondence should be addressed. Electronic mail: thomas.yankeelov@vanderbilt.edu

[1]I. Khalkhali, I. Mena, and L. Diggles, "Review of imaging techniques for the diagnosis of breast cancer: A new role of prone scintimammography using technetium-99m sestamibi," Eur. J. Nucl. Med. **21**, 357–362 (1994).
[2]K. Yutani, M. Tatsumi, T. Uehara, and T. Nishimura, "Effect of patients' being prone during FDG PET for the diagnosis of breast cancer," Am. J. Roentgenol. **173**, 1337–1339 (1999).
[3]H. Kaida, M. Ishibashi, T. Fuji, S. Kurata, M. Uchida, K. Baba, T. Miyagawa, H. Kaibara, S. Kawamura, E. Ogo, and N. Hayabuchi, "Improved breast cancer detection of prone breast fluorodeoxyglucose-PET in 118 patients," Nucl. Med. Commun. **29**, 885–893 (2008).
[4]L. Moy, M. E. Noz, G. Q. Maguire, Jr., A. Melsaether, A. E. Deans, A. D. Murphy-Walcott, and F. Ponzo, "Role of fusion of prone FDG-PET and magnetic resonance imaging of the breasts in the evaluation of breast cancer," Breast J. **16**, 369–376 (2010).
[5]L. Moy, F. Ponzo, M. E. Noz, G. Q. Maguire, Jr., A. D. Murphy-Walcott, A. E. Deans, M. T. Kitazono, L. Travascio, and E. L. Kramer, "Improving specificity of breast MRI using prone PET and fused MRI and PET 3D volume datasets," J. Nucl. Med. **48**, 528–537 (2007).
[6]R. G. Abramson, K. F. Lambert, L. B. Jones-Jackson, L. R. Arlinghaus, J. M. Williams, V. G. Abramson, A. B. Chakravarthy, and T. E. Yankeelov, "Prone

Versus Supine Breast FDG-PET/CT for Assessing Locoregional Disease Distribution in Locally Advanced Breast Cancer," Acad. Radiol. (2015) [epub ahead of print].
[7]X. Li, R. G. Abramson, L. R. Arlinghaus, A. B. Chakravarthy, V. Abramson, I. Mayer, J. Farley, D. Delbeke, and T. E. Yankeelov, "An algorithm for longitudinal registration of PET/CT images acquired during neoadjuvant chemotherapy in breast cancer: Preliminary results," EJNMMI Res. **2**, 62 (2012).
[8]N. C. Atuegwu, X. Li, L. R. Arlinghaus, R. G. Abramson, J. M. Williams, A. B. Chakravarthy, V. G. Abramson, and T. E. Yankeelov, "Longitudinal, intermodality registration of quantitative breast PET and MRI data acquired before and during neoadjuvant chemotherapy: Preliminary results," Med. Phys. **41**, 052302 (5pp.) (2014).
[9]R. L. Wahl, H. Jacene, Y. Kasamon, and M. A. Lodge, "From RECIST to PERCIST: Evolving considerations for PET response criteria in solid tumors," J. Nucl. Med. **50**(1), 122S–150S (2009).
[10]S. Beaulieu, P. Kinahan, J. Tseng, L. K. Dunnwald, E. K. Schubert, P. Pham, B. Lewellen, and D. A. Mankoff, "SUV varies with time after injection in (18)F-FDG PET of breast cancer: Characterization and method to adjust for time differences," J. Nucl. Med. **44**, 1044–1050 (2003).
[11]FDG-PET/CT Technical Committee, FDG-PET/CT as an imaging biomarker measuring response to cancer therapy profile, Quantitative Imaging Biomarkers Alliance, version 1.05, publicly reviewed version, 11 December 2013, available http://rsna.org/QIBA.aspx.
[12]A. K. Tahari and R. L. Wahl, "Quantitative FDG PET/CT in the community: Experience from interpretation of outside oncologic PET/CT exams in referred cancer patients," J. Med. Imaging Radiat. Oncol. **58**, 183–188 (2014).
[13]J. A. Thie, K. F. Hubner, and G. T. Smith, "Optimizing imaging time for improved performance in oncology PET studies," Mol. Imaging Biol. **4**, 238–244 (2002).
[14]C. Y. Wong, D. Noujaim, H. F. Fu, W. S. Huang, C. Y. Cheng, J. Thie, I. Dalal, C. Y. Chang, and C. Nagle, "Time sensitivity: A parameter reflecting tumor metabolic kinetics by variable dual-time F-18 FDG PET imaging," Mol. Imaging Biol. **11**, 283–290 (2009).
[15]A. R. Stahl, T. A. Heusner, V. Hartung, J. Nagarajah, A. Bockisch, S. Hahn, G. Antoch, and W. Jentzen, "Time course of tumor SUV in 18F-FDG PET of breast cancer: Presentation of a simple model using a single reference point for time corrections of tumor SUVs," J. Nucl. Med. **52**, 18–23 (2011).
[16]J. van den Hoff, A. Lougovski, G. Schramm, J. Maus, L. Oehme, J. Petr, B. Beuthien-Baumann, J. Kotzerke, and F. Hofheinz, "Correction of scan time dependence of standard uptake values in oncological PET," EJNMMI Res. **4**, 18 (2014).
[17]L. K. Shankar, J. M. Hoffman, S. Bacharach, M. M. Graham, J. Karp, A. A. Lammertsma, S. Larson, D. A. Mankoff, B. A. Siegel, A. Van den Abbeele, J. Yap, and D. Sullivan, "Consensus recommendations for the use of 18F-FDG PET as an indicator of therapeutic response in patients in National Cancer Institute trials," J. Nucl. Med. **47**, 1059–1066 (2006).
[18]D. Delbeke, R. E. Coleman, M. J. Guiberteau, M. L. Brown, H. D. Royal, B. A. Siegel, D. W. Townsend, L. L. Berland, J. A. Parker, K. Hubner, M. G. Stabin, G. Zubal, M. Kachelriess, V. Cronin, and S. Holbrook, "Procedure guideline for tumor imaging with 18F-FDG PET/CT 1.0," J. Nucl. Med. **47**, 885–895 (2006).
[19]J. Kalpathy-Cramer, J. B. Freymann, J. S. Kirby, P. E. Kinahan, and F. W. Prior, "Quantitative imaging network: Data sharing and competitive algorithm validation leveraging the cancer imaging archive," Transl. Oncol. **7**, 147–152 (2014).
[20]L. I. Lin, "A concordance correlation coefficient to evaluate reproducibility," Biometrics **45**, 255–268 (1989).
[21]J. M. Williams, S. D. Rani, X. Li, J. G. Whisenant, H. Kang, L. Arlinghaus, A. B. Chakravarthy, V. Abramson, R. Abramson, and T. E. Yankeelov, "Prone versus supine 18F-FDG-PET for assessing the response of locally advanced breast cancer to neoadjuvant chemotherapy," The Journal of Nuclear Medicine **55**(Suppl. 1), 1519 (2014), available at http://jnumedmtg.snmjournals.org/cgi/content/short/55/1_MeetingAbstracts/1519.
[22]See supplementary material at http://dx.doi.org/10.1118/1.4921363 for individual patient demography and disease characteristics as well as individual lesion SUVpeak and SUVmax measurements in prone versus supine 18F-FDG-PET.